

# Large-scale drivers of Caucasus climate variability in meteorological records and Mt Elbrus ice cores

Anna Kozachek<sup>1,2,3</sup>, Vladimir Mikhalenko<sup>2</sup>, Valérie Masson-Delmotte<sup>3</sup>, Alexey Ekaykin<sup>1,4</sup>, Patrick Ginot<sup>5,6</sup>, Stanislav Kutuzov<sup>2</sup>, Michel Legrand<sup>5</sup>, Vladimir Lipenkov<sup>1</sup>, Susanne Preunkert<sup>5</sup>

1. Climate and Environmental Research Laboratory, Arctic and Antarctic Research Institute, Saint Petersburg, 199397, Russia

2. Institute of Geography, Russian Academy of Sciences, Moscow, 119017, Russia

3. Laboratoire des Sciences du Climat et de l'Environnement, CEA/CNRS/UVSQ/IPSL, Gif-sur-Yvette, 91191, France

4. Institute of Earth Sciences, Saint Petersburg State University, Saint Petersburg, 199178, Russia

5. Laboratoire de Glaciologie et Géophysique de l'Environnement, CNRS/UGA, Grenoble, 38400, France

6. Observatoire des Sciences de l'Univers de Grenoble, IRD/UGA/CNRS, Grenoble, 38400, France

*Correspondence to:* Anna Kozachek (kozachek@aari.ru)

## Abstract

A 181.8 m ice core was recovered from a borehole drilled into bedrock on the western plateau of Mt. Elbrus (43°20'53.9'' N, 42°25'36.0'' E; 5115 m a.s.l.) in the Caucasus, Russia, in 2009 (Mikhalenko et al., 2015). Here, we report on the results of the water stable isotope composition from this ice core with additional data from the shallow cores.. There is a distinct seasonal cycle of the isotopic composition which allowed dating by annual layer counting. Dating has been performed for the upper 126 m of the deep core combined with 20 m from the shallow cores.. The whole record covers 100 years from 2013 back to 1914. Due to the high accumulation rate (1380 mm w.e. per year) and limited melting we obtained the isotopic composition and accumulation rate records with seasonal resolution. These values were compared with available meteorological data from 13 weather stations in the region, and also with atmosphere circulation indices, back-trajectories calculations and GNIP data in order to decipher the drivers of accumulation and ice core isotopic composition in the Caucasus region. In the warm season (May - October) the isotopic composition depends on the local temperature, but the correlation is not persistent in time, while in cold season (November – April), the atmospheric circulation is the predominant driver of the ice core isotopic composition. The snow accumulation rate correlates well with the precipitation rate in the region all year round, this made it possible to reconstruct and expand the precipitation record at the Caucasus highlands from 1914 till 1966 when the reliable meteorological observations of precipitation at high elevation began.

## 1 Introduction

36 Large scale modes of variability such as the NAO (North Atlantic Oscillation) are known to influence European climate  
37 variability (see review in Panagiotopoulos et al., 2002). However, most studies of large-scale drivers of European climate  
38 change have been focused on low elevation instrumental records from weather stations, and there is very limited information  
39 about climate variability at high altitudes, and about differences in climate variability and trends at different elevations  
40 (EDW research group, 2015). Such differences were calculated in many mountain regions (EDW research group, 2015),  
41 except for the Caucasus, due to the lack of high elevation instrumental observations in this region.

42 The Caucasus is located southwards of the East European Plain. It is a high mountain region, with typical elevations of 3200-  
43 3500 m a.s.l., and with the highest point reaching 5642 m for Elbrus. The Main Caucasus Ridge acts as a barrier between  
44 subtropical and temperate mid-latitude climates, as observed for other high mountain regions such as the Himalaya. As in  
45 other mountain regions, there is a lack of high elevation meteorological records in the Caucasus. Moreover, existing records  
46 are relatively short: for example, reliable Caucasus precipitation measurements started only in 1966. An improved spatio-  
47 temporal coverage is required to investigate internal variability, to explore trends and spatial differences, and to evaluate the  
48 skills of atmospheric models providing atmospheric analysis products where no meteorological data are assimilated.

49 Measurements of the stable isotope composition of water, and annual accumulation rates in mid to high latitude ice cores are  
50 widely used proxies to estimate past temperature and precipitation rate changes. In many high mountain regions such as the  
51 Caucasus, and for elevations situated above the tree line, ice core data provides the only source of detailed information to  
52 document past climate changes, complementing punctual information retrieved from changes in glacier extent and recent  
53 glacier mass balance. For example study of the water stable isotope composition of several ice cores obtained in the Alps  
54 was recently conducted by Mariani et al. (2014) and the same research in Alaska was performed by Tsushima et al. (2015).  
55 The authors explored the links between the ice cores isotopic composition, local climate and large-scale circulation patterns.  
56 They found that in mountain regions isotopic composition of the ice cores governed both by the local meteorological  
57 conditions and by the regional and global factors. These studies discussed the complexity of interpreting ice core records  
58 from high-altitude glaciers due to the potential bias from post-depositional processes and frequent changes in the origin of  
59 moisture sources. For instance, even in areas without any seasonal melt, accumulation is the net effect of precipitation,  
60 sublimation, and wind erosion processes, and may significantly differ from precipitation. Water stable isotope records are in  
61 mid to high latitudes physically related to condensation temperature through distillation processes (Dansgaard, 1964), but the  
62 climate signal is archived through the snowfall deposition and post-deposition processes. One important artefact lies in the  
63 intermittency of precipitation, and the covariance between condensation temperature and precipitation, which may bias the  
64 climate record towards one season, or towards one particular weather regime, challenging an interpretation in terms of  
65 annual mean temperature (Persson et al., 2011). Moreover, water stable isotopes are integrated tracers of all phase changes  
66 occurring from evaporation to mountain condensation, and are also affected by non-local processes related to evaporation  
67 characteristics, or shifts in initial moisture sources. Such processes have the potential to alter the validity of an interpretation  
68 of the proxy record in terms of local, annual mean, or precipitation-weighted temperature. In some region, isotopic records  
69 are more related to hydrological cycles, recycling, rainout (Aemisegger et al., 2014). Finally, the condensation temperature

70 may also strongly differ from surface air temperature; depending on elevation shifts in e.g. planetary boundary layer or  
71 convective activity (see Ekaykin and Lipenkov, 2009 for a review). While these processes make the interpretation of ice core  
72 records complex, they conversely open the possibility that the ice core proxy record may be in fact more sensitive to large-  
73 scale climate variability than punctual precipitation amounts. For instance, Casado et al (2014) have evidenced a strong  
74 fingerprint of the NAO in water stable isotope records from central Western Europe and Greenland, either in long  
75 instrumental records based on precipitation sampling, in seasonal ice core records, or in atmospheric models including water  
76 stable isotopes. Connection of Greenland ice cores isotopic composition with the atmospheric circulation patterns was  
77 studied by Vinther et al. (2003 and 2010). The strong influence of the NAO pattern on the Greenland ice cores isotopic  
78 composition has been discovered and the possibility to use the ice cores data for the past NAO changes reconstruction was  
79 proved (Vinther et al., 2003). The authors also revealed the importance of the seasonally resolved ice cores records study  
80 rather than annual records as there are different factors governing formation of the isotopic composition of precipitation in  
81 warm and in cold seasons (Vinther et al., 2010).

82 We will now briefly review earlier studies performed on climate variability in the Caucasus area, and which have already  
83 explored the relationships between regional climate, glacier expansion, and large-scale modes of variability: the NAO (North  
84 Atlantic Oscillation), AO (Arctic Oscillation), and NCP (North Sea – Caspian Pattern). For example, Shahgedanova et al.  
85 (2005) monitored the mass balance of the Djankuat glacier, situated at an altitude between 2700 and 3900 m a.s.l. While no  
86 significant correlation was identified between accumulation rate and the winter NAO index, the years of high accumulation  
87 systematically occurred during winters with a very negative NAO index. Brunetti et al. (2011) explored the influence of the  
88 NCP mode on climate in Europe and around the Mediterranean region. They evidenced a negative correlation coefficient of -  
89 0.50 between temperature in the Caucasus and the NCP index. Baldini et al. (2008) investigated records of precipitation  
90 isotopic composition in Europe from the IAEA/GNIP stations, extrapolating a significant negative correlation between  
91 winter precipitation  $\delta^{18}\text{O}$  in the Caucasus region and the NAO index ( $R = -0.50$ ). Casado et al (2013) studied the influence  
92 of precipitation intermittency on the relationships between precipitation  $\delta^{18}\text{O}$ , temperature, and the NAO. The influence of  
93 the NAO index on European climate and precipitation  $\delta^{18}\text{O}$  appeared more prominent in winter than in summer (Comas-Bru  
94 et al., 2016).

95 Here, we take advantage of the new Elbrus deep ice cores (Mikhalevko et al., 2015), and produce the first analysis of water  
96 stable isotope and accumulation records. Section 2 introduces the data and methods, with a description of the ice core  
97 analyses and age scale, an overview of regional meteorological information, as well as the source of information for indices  
98 of modes of variability. Section 3 presents the results of the comparison and statistical analyses of the relationships between  
99 regional climate parameters (temperature and precipitation), Elbrus ice core records, and modes of variability. In section 4,  
100 we finally summarize our key findings and the next steps envisaged to strengthen the climatic interpretation of the Caucasus  
101 ice core records.

## 102 **2 Data and methods**

103

104  
105  
106  
107  
108  
109  
110  
111  
112  
113  
114  
115  
116  
117  
118  
119  
120  
121  
122  
123  
124  
125  
126  
127  
128  
129  
130  
131  
132  
133  
134  
135  
136  
137

**2.1 Ice core data**

**2.1.1 Drilling site and drilling campaigns**

Here, we report on results from the new, deepest ice core from Mt Elbrus, in comparison with results from shallow ice cores. Deep drilling was performed on the Western Plateau (43°20'53.9" N, 42°25'36.0" E; 5115 m a.s.l.) of Mt Elbrus (fig. 1) in September 2009, allowing recovery of a 181.8 m long ice core, down to bedrock. The drilling site and the drilling operations are thoroughly described in Mikhalenko et al. (2015).

In order to update the ice core records towards the present-day, and enable a comparison of the measurements with local meteorological monitoring data, surface drilling operations were repeated at the same place in 2012 (11.5 m long) and in 2013 (20.5 m long). Results are also compared here with previously published isotopic composition data measured along the 22 m shallow ice core drilled at the same place in 2004 which covered the period from 1998 till 2004. (Mikhalenko et al, 2005).

In 2014, drilling operations were also successful at the Maili Plateau (Mt. Kazbek), at the altitude of 4500 m a.s.l. in 200 km eastwards from Elbrus (fig. 1), delivering a 20-m ice core. The Kazbek core is shown for the comparison only. Its detailed description will be published elsewhere.

**2.1.2 Sampling process and sampling resolution**

For the upper and the lower parts of the deep core (0-106 m and 158-181.8 m) and for the shallow firn cores drilled in 2012 and 2013, sampling was performed using classical cutting-melting procedures. For the other depth intervals, melted samples were extracted from the continuous flow analysis system of LGGE (Grenoble, France), automatically sub-sampled, frozen and stored in vials for subsequent isotopic analysis. The description of the CFA system will be published elsewhere.

The sampling resolution was 15 cm for the upper 16 m of the deep core (see the sketch of the sampling resolution in fig. 2c). It was then increased to 5 cm in order to achieve better resolution, from 16 to 70 m depth and in the bottom part of the core (158-182 m depth). To ensure 15-20 samples per year, the sampling resolution was increased to 4 cm in the depth range from 70 to 106 m, similar to the sampling resolution of the CFA system (3.7 cm).

Samples from the shallow cores drilled in 2012 and 2013 were cut with a resolution of 10 and 5 cm, respectively.

**2.1.3 Isotopic measurements**

The methods of the isotopic measurements have been partially discussed in (Mikhalenko et al., 2015). Water stable isotope ratios ( $\delta^{18}\text{O}$  and  $\delta\text{D}$ ) were measured at the Climate and Environmental Research Laboratory (CERL) of Arctic and Antarctic

138 research Institute (St Petersburg, Russia), using a Picarro L2120-i analyzer. Each sample was measured once. Sequences of  
139 measurements included the injection of 5 samples, followed by the injection of an internal laboratory standard with an  
140 isotopic value close to that of the samples. We also repeated the measurements of about 10% of all the samples in order to  
141 calculate the analytical precision: 0.06‰ for  $\delta^{18}\text{O}$  and 0.30‰ for  $\delta\text{D}$ . The depth profile of  $\delta^{18}\text{O}$  (Mikhaleenko et al., 2015;  
142 Kozachek et al., 2015) and of the deuterium excess ( $d = \delta\text{D} - 8 \cdot \delta^{18}\text{O}$ ) are shown in fig. 2.  
143 Moreover, 600 samples from the depth interval from 23 to 35 m were measured in the Laboratory of Isotope Hydrology of  
144 the IAEA (Vienna, Austria). The two records are highly correlated ( $r=0.99$ ,  $p < 0.05$ ) for both isotopes (Figure S2b) with a  
145 systematic offset of 0.2 ‰ for  $\delta^{18}\text{O}$  and 1 ‰ for  $\delta\text{D}$ . The records of the second order parameter deuterium excess are also  
146 significantly correlated ( $r=0.65$ ,  $p < 0.05$ ) without any specific trend or systematic offset. This inter-laboratory comparison  
147 demonstrates the high quality of the isotopic measurements performed in CERL.  
148 We also stress the close overlap of the upper part of the profiles of the water stable isotope records versus depth from the  
149 different cores drilled in 2009, 2012 and 2013 (Fig. S2a). Based on this close agreement within the different shallow firn  
150 cores, we decided to calculate a stack record for the period from 1914 till 2013 which is used hereafter for the dating.  
151 In the depth interval from 100 to 106 m depth, we also have an overlap of samples obtained with classical cutting method  
152 and CFA method described above, without any significant difference (Fig. S2c), again allowing us to combine the two  
153 records into one stack record.

154

#### 155 **2.1.4 Dating**

156

157 The chronology is based on the identification of annual layers. These are prominent in  $\delta^{18}\text{O}$  with the average seasonal  
158 amplitude of 20 ‰. For annual mean values we calculated averages of  $\delta^{18}\text{O}$  from one minimum of this parameter to another  
159 one as well as from one maximum to another. As we found no significant differences between the records obtained with two  
160 ways of year allocation we use minimum to minimum dating as more common one. We compared annual layers counting  
161 performed independently using the seasonal cycles in the isotopic composition and the ammonium concentration. The  
162 discrepancy between two independent chronologies is 2 years at a depth of 126 m. We used the dating based on the isotopic  
163 composition data in this paper. This dating is also best fit for the correlation analysis with the meteorological data. Hereafter,  
164 we focus our analysis on one century, from 1914 till 2013, which corresponds to the upper 126 m of the core. This period has  
165 been chosen because of relatively small dating uncertainty and the availability of other records such as local meteorological  
166 observations. At the bottom part of the core the isotopic composition cycles are less prominent and cannot be used for dating,  
167 consequently the dating uncertainty is sufficiently higher. The isotopic composition of that part of the core will be discussed  
168 elsewhere. In meteorological data we used average values from January to December of each year for the comparison with  
169 annual means of ice cores parameter.

170 For warm and cold seasons allocation we used slightly adapted method from (Vinther et al., 2010). The original method  
171 requires ascribing of equal accumulation rate for warm and cold season of each year. We changed the borders between the

172 seasons when needed in order to avoid ascribing minimum of  $\delta^{18}\text{O}$  to the warm season and maximum to the cold season.  
173 We stacked to keeping the extreme values in the middle of the season as this is in coherence with meteorological data. We  
174 also used ammonium concentration as an independent marker, using criteria described on (Mikhalenko et al., 2015). For  
175 equivocal situations, we also used additional data: melt layers and dust layers (used to identify the warm season) (Kutuzov et  
176 al., 2013) as well as succinic acid concentration data that also have seasonal variations (Mikhalenko et al., 2015).

177 Figure 3 illustrates the identification of seasons using the isotopic composition seasonal cycle. In meteorological data we  
178 used period from November to April for the cold season and period from May to October for the warm season.

179 There some gaps in the isotopic composition data that came from the technical problems during the drilling operations and  
180 the analysis process. The drilling problems are described in (Mikhalenko et al., 2015). The biggest gap appears at the depth  
181 31.3 and 32.1 m. There was a piece of the core lost during the drilling operations. This part is covered by the bottom part of  
182 the 2004 core where the sampling resolution was 50 cm. It is evident that two seasons (one warm and one cold) are partially  
183 missing. We didn't use these values for the correlation analysis because of large uncertainty of the seasonal values  
184 calculations in this case. In case of one sample missing we considered its isotopic value to be the average between the two  
185 neighbor samples. For a detailed description of the raw isotopic data and annual layers allocation for the upper 106 m of the  
186 core, please refer to Mikhalenko et al. (2015). Mean annual and seasonal values of  $\delta^{18}\text{O}$  and  $d$  obtained as a result of the  
187 dating are shown in fig. 5 and 6 respectively.

188 The annual accumulation rate is calculated as the thickness of the seasonal layer, multiplied by the layer density using the  
189 density profile from Mikhalenko et al. (2015), and corrected for layer thinning using the Dansgaard-Johnsen model  
190 (Dansgaard and Johnsen, 1969), with the following parameters: accumulation rate 1.583 m of ice equivalent, pore close-off  
191 depth = 55 m (Mikhalenko et al., 2015).

### 193 **2.1.5 Diffusion of stable isotopes**

194  
195 We calculated the potential influence of diffusion on the stable isotopes record according to (Johnsen, 2000) model. We used  
196 the following parameters for the calculation: Our calculation showed that the seasonal amplitude of  $\delta^{18}\text{O}$  variations could be  
197 10-20% less because of the diffusion (Mikhalenko et al., 2015). If it was the case we would observe a decreasing of  $\delta^{18}\text{O}$   
198 maxima and increasing of minima with depth. Moreover we would find a positive correlation between layer thickness and  
199 seasonal amplitude of  $\delta^{18}\text{O}$ . These features have not been found in the ice core data. The correlation coefficient between  
200 seasonal amplitude and accumulation rate is -0.10 and is statistically insignificant. There is also no statistically significant  
201 trend in the seasonal amplitude; the seasonal amplitude varies stochastically from 10 to 25 %. The maximum value observed  
202 on 1984 and the minimum in 1925. We therefore consider that the diffusion does not influence sufficiently the isotopic  
203 composition record in the upper 126 m of the ice core. At the bottom part of the core (e.g. at a depth of 180 m) the annual  
204 cycle of  $\delta^{18}\text{O}$  should have an amplitude of 4 ‰ which is detectable but the length of the cycle should be less than 1 cm. As

205 the  $d$  annual cycle is not prominent we cannot use the method based on the discrepancy between the  $\delta^{18}\text{O}$  and  $d$  cycles.  
206 Thus, for obtaining climatic information from the bottom part of the core very high sampling resolution is required.

207

## 208 **2.2 Meteorological data**

209

210 We used the daily meteorological data (precipitation rate and mean daily temperature) from several weather stations around  
211 the drilling site (see map in Fig. 1 and Table 1) for comparison with the ice core data. We also investigated records of  
212 precipitation isotopic composition based on monthly sampling, performed at three stations to the south of Caucasus within  
213 the WMO-IAEA Global Network of Isotopes in Precipitation (GNIP) program (Table 1).

214 For comparison we used the NCEP/NCAR reanalysis temperature data (Kalnay et al., 1996) for the 500 mbar level which  
215 corresponds to the drilling site altitude. Two different models were used to calculate back trajectories: FLEXPART (Forster  
216 et al., 2007, Stohl et al., 2009), HYSPLIT (Draxler, 1999, Stein et al., 2015, Rolph, 2016). The LMDZiso model was used to  
217 estimate the precipitation isotopic composition at the drilling site (Risi et al., 2010).

218

## 219 **2.3. Circulation indices**

220 Circulation of the atmosphere influences sufficiently isotopic composition of the ice cores (Casado et al., 2013 and references  
221 therein). Atmospheric circulation is quantitatively characterized by circulation indices. In this research we used three indices:  
222 NAO, AO, NCP that are widely used to characterize European climate (Jones et al., 2003, Thompson and Wallace, 2001,  
223 Brunetti et al., 2011 and references therein). Time span and references for the indices are presented in table 1.

224 NAO (North-Atlantic Oscillation) characterizes type of circulation in Europe, strength of Azores maximum and Icelandic  
225 minimum. Positive values of NAO index correspond to lower than usual value of atmospheric pressure in Iceland and higher  
226 than usual value of atmospheric pressure at Azores. Negative index corresponds to less prominent centers of action in the  
227 Northern Hemisphere. Usually this index is calculated as difference of atmospheric pressure measured at Reykjavik and  
228 Lisbon, Ponta Delgada or Gibraltar. Here we used data from (Vinther et al., 2003 and  
229 <https://crudata.uea.ac.uk/~timo/datapages/naoi.htm>) that were calculated using data from Gibraltar station. Negative NAO  
230 leads to increase of precipitation rate in Southern Europe, positive NAO leads to increase of precipitation rate in Northern  
231 Europe (Hurrell, 1995, Jones et al., 2003, Vinther et al., 2003).

232 Arctic Oscillation index (AO) also is a characteristic of the Northern Hemisphere circulation. It is used to analyze climatic  
233 variability with periods longer than 10 years. It is calculated as EOF of 500 hPa surface. Negative values correspond to high  
234 pressure at the Pole and cooling of Europe, while positive values correspond to low pressure at the Pole and drying of  
235 Mediterranean (Thompson and Wallace, 2001). We used AO data from NOAA  
236 (<http://www.cpc.ncep.noaa.gov/products/precip/CWlink/>).

237 NCP (North-Sea Caspian Pattern) index is less widely used, though it was proved that it is convenient to use it in  
238 Mediterranean climate studies (Kutiel et al., 1997; Brunetti et al., 2011). The index is calculated as normalized difference of

239 geopotential heights between Caspian and Northern seas. Positive values correspond to stronger meridional circulation in  
240 Europe and lower summer temperatures, Negative values reflect strengthening of zonal circulation and higher summer  
241 temperatures in Europe (Brunetti et al., 2011). We used NCP data from NOAA  
242 (<http://www.cpc.ncep.noaa.gov/products/precip/CWlink/>).

## 244 **3 Results**

### 246 **3.1 Regional climate**

248 The main peculiarity of the drilling site is its location on the border between subtropical and temperate climatic zones  
249 (Volodicheva, 2004). Back-trajectory calculations show that the drilling site is characterized by remarkable seasonal  
250 differences in moisture sources locations. In winter, the origin of air masses varies from the Mediterranean to the North  
251 Atlantic. In summer, local moisture sources from the surrounding continents or from the Black Sea are predominant (see fig.  
252 S1 for examples).

253 Meteorological data depict large regional variations in the seasonal cycle of precipitation. To the south of the Caucasus, there  
254 is no distinct seasonal cycle (Fig. 4a), showing the climatology for the Klukhorskyy Pereval station. In fact, the Klukhorskyy  
255 Pereval station is situated north of the Main ridge, but in terms of the seasonal cycle of precipitation it undoubtedly belongs  
256 to the southern group. But we are nevertheless using this station as an example because of the uninterrupted record of  
257 temperature and precipitation for the 1966-1990 period. By contrast, the north of the Caucasus is marked by a distinct  
258 seasonality in precipitation amounts, which are maximum in summer and minimum in winter (Fig. 4b), showing the  
259 climatology for the Mineralnye Vody station. More examples of the Caucasus weather stations climatologies are given in  
260 (Mikhaleiko et al., 2015). Moreover, the annual precipitation rate to the south of the Caucasus is much higher than to the  
261 north. For example, the typical annual precipitation rate to the north of the Caucasus at the altitude close to the sea level is  
262 500 mm per year, while to the south of the Caucasus at the same altitude it is about 1500 mm. The amount of precipitation in  
263 the region is affected by the altitude and the distance from the sea shore.

264 The seasonal changes of temperature appear uniform all over the region surrounding Caucasus, with warmest conditions  
265 observed in summer and coldest conditions observed in winter. The seasonal amplitude depends on the distance from the sea  
266 and the mean annual temperature depends on the altitude. The average regional lapse rate was calculated using the available  
267 meteorological data, we used the data from all of the stations for the calculation. The lapse rate is lowest in winter (2.3°C per  
268 1000 m) and highest (5.2 °C per 1000 m) in summer (Fig. S3).

269 Based on the lapse rate we calculated temperature at the drilling site (see Fig.8a for the annual mean temperature variations.  
270 and 8b and 8c for seasonal records). For precipitation data, available in this region since 1966, we show all the data (fig. S4),  
271 while in the calculations we used data from Klukhorskyy Pereval station as an example of stations without a seasonal cycle  
272 and Mineralnye Vody station as an example of those with a prominent cycle. More examples of annual variations of



273 temperature and precipitation at the Caucasus meteorological stations can be found in (Shahgedanova et al., 2014) and  
274 (Tielidze, 2016). At our drilling site, an automatic weather station (AWS) provided in situ measurements for the period from  
275 August 2007 till January 2008. The day to day variations of temperature at low elevation weather stations and at the AWS  
276 are coherent for the whole period of the AWS work (Mikhalenko et al., 2015).

277 We also compared the data from meteorological stations with the NCEP reanalysis (Kalnay et al., 1996) outputs (not shown)  
278 for the 500 mbar level. Despite difference in absolute values on the daily scale when compared with the AWS data (the  
279 difference is random and varies from -1 to 1 °C), the observed regional data and reanalysis data have the same month to  
280 month variability. The maximum daily mean temperature at the drilling site according to the reanalysis data was -1.3 °C for  
281 the whole dataset. The temperature in the glacier at 10m depth, which correspond to the annual mean temperature at the  
282 drilling altitude, is -17 °C (Mikhalenko et al., 2015), the annual mean temperature at the drilling altitude from the NCEP  
283 reanalysis is -14 °C, and the same value calculated from meteorological observations and corrected for the lapse rate is -11  
284 °C.

285 We then investigated long-term trends in the meteorological records. Mean annual temperatures show significant increase  
286 during last two decades. We also observe higher than average values of mean decadal temperature in 1930-1940. And the  
287 beginning of the observations in the region, i.e. period from 1881 till 1900 was as cold as the 1990s. It is evident that last 20  
288 years in warm season were the warmest for the whole observation period (fig. 8), while in cold the recent warming is not  
289 unprecedented. For example, cold seasons in the 1960s – 1970s were even warmer (fig. 8). Multi-decadal patterns of  
290 temperature variations also differ in the late 19<sup>th</sup> Century, where negative anomalies are identified in cold season temperature  
291 (Fig. 8) but not in warm season temperature (Fig 8). On the other hand in cold season temperatures we can observe lower  
292 temperatures at the end of 19<sup>th</sup> century that can be impact of the volcanic eruptions (Stoffel et al., 2015). We also noted the  
293 high temperature values in the 1910s - 1920s that is not completely understood. We did not find any trends in the  
294 precipitation rate for neither of the groups of stations (fig. S4).

295 A significant anti-correlation is observed between temperature and the NAO index, both in cold and warm seasons (Table 2,  
296 the information about the time series used for the correlation analysis can be found in Table 1). Stronger anti-correlations are  
297 identified between temperature and the NCP index, especially in cold season, as also reported by Brunetti et al. (2011).  
298 Relationships with indices of large scale modes of variability are systematically weaker for precipitation, with contradictory  
299 results for the south\north Caucasus stack; they appear significant for the NCP in both seasons (Table 2).

300 GNIP data are only available at low elevation stations. They show a rather uniform distribution of the isotopic composition  
301 of precipitation in the region during summer, as well as a gradual depletion of  $\delta^{18}\text{O}$  at higher altitudes in winter.

302 GNIP records are too short and intermittent (one-two years with gaps) to investigate the variability and relationships with the  
303 local temperature on interannual scale. We therefore restrict discussion of GNIP data to seasonal variations. The  $\delta^{18}\text{O}$  and  $\delta\text{D}$   
304 in precipitation have a distinct seasonal cycle with maximum values observed in warm season (JJA) and minimum values  
305 observed in cold season (DJF). As an example we show the seasonal cycle of  $\delta^{18}\text{O}$  and  $d$  for Bakuriani station in 2009 (fig.  
306 7). This station is the only one in the region for which the whole uninterrupted dataset for one annual cycle is available. The

307 seasonal amplitude of  $\delta^{18}\text{O}$  is about 17 ‰. The slope between  $\delta^{18}\text{O}$  and temperature is 0.32 ‰/°C. The  $d$  variations show no  
308 seasonal cycle varying randomly between 10 ‰ and 25 ‰. We found no significant correlation between  $\delta^{18}\text{O}$  and  $d$ .  
309 Climate variability as a driver for glacier variations in the Caucasus has recently been explored by several authors.  
310 Elizbarashvili et al. (2013) found the increased frequency of extremely hot months during the 20th century, especially over  
311 Eastern Georgia, whereas number of extremely cold months decreased faster in the Eastern than in the Western region. In  
312 addition, highest rates for positive trends of annual mean air temperature can be observed in the Caucasus Mountains.  
313 Shahgedanova et al. (2014) evidenced significant glacier recession at the northern slopes of the Caucasus, consistent with  
314 increasing air temperature of the ablation season. They report that the most recent decade (2001-2010) was 0.7 – 0.8 °C  
315 warmer than in 1960-1986 at Terskol and Klukhorskiy Pereval stations (see Table 1 for information on stations). However,  
316 the warmest decade for JJA was 1951-1960 (Shahgedanova et al., 2014). Tielidze (2016) reports recent increase of the  
317 annual mean temperatures at different elevations in the Georgian Caucasus. The region experienced glacier area loss over the  
318 20<sup>th</sup> century at an average annual rate of 0.4% with a higher rate in eastern Caucasus than in the central and western sections.  
319 The analysis of temperature and radiation regime of glaciers at the ablation period has been performed at Elbrus vicinities  
320 recently (Toropov et al., 2016). The authors prove that the observed waning of glaciers cannot be explained by increase of  
321 temperature during the ablation period because of increase of precipitation during the accumulation period. They concluded  
322 that the main driver of glacier retreat is increase of the solar radiation balance for 4% for the 2001-2010 period which  
323 corresponds to increase of ablation for 140 mm per ablation season (Toropov et al., 2016).

324

### 325 **3.2 Ice core records**

326

327 The comparison of the four cores obtained at the Western Plateau of Elbrus shows similar variations during overlap periods  
328 (see Fig. 2S). We therefore calculate a stack record for each season, based on the average value of individual ice cores for the  
329 overlapping seasons. The inter-core disagreement is almost negligible (fig. 2S) and can be explained by different sampling  
330 resolution.

331 We note that the shallow ice core from the Maili plateau of Kazbek shows the same mean values of  $\delta^{18}\text{O}$  as the Elbrus ice  
332 cores during their overlap period. This is a result of a mutual compensation of  $\delta^{18}\text{O}$  increase due to lower elevation position  
333 (Kazbek drilling site is 500 m lower) and of  $\delta^{18}\text{O}$  decrease because of continentality effect (Kazbek is 200 km further from  
334 the sea). The inter-annual variability in isotopic composition is about twice larger in cold season than in warm season for  
335  $\delta^{18}\text{O}$ . Different patterns of inter-annual to multi-decadal variations appear in the instrumental temperature data (see section  
336 3.1) and ice core  $\delta^{18}\text{O}$  records (Fig 5) emerge for cold versus warm season.

337 The  $\delta\text{D}$  and  $\delta^{18}\text{O}$  values are highly correlated ( $r = 0.99$ ) on sample to sample scale so hereafter we use the  $\delta^{18}\text{O}$  information  
338 for the dating and comparison with the other parameters. The slope between  $\delta^{18}\text{O}$  and  $\delta\text{D}$  is 8.03 on sample to sample scale  
339 and 7.9 on seasonal scale without any significant difference between the two seasons.

340 No significant (R squared is insignificant at  $p < 0.05$ ) centennial trend is identified in cold / warm season  $\delta^{18}\text{O}$ , nor in cold /  
341 warm season accumulation rate or deuterium excess. We observe large variations in  $\delta^{18}\text{O}$  with high and variable values early  
342 20<sup>th</sup> century, lower and more stable values in the 1940s-1960s, and a step increase in the 1970s with another level. These  
343 variations are coherent in both seasons as well as in annual means but are not reflected in the meteorological observations.  
344 There is also an increase of  $\delta^{18}\text{O}$  in the last two decades in both seasons in regard to the 1970s-1980s values but the absolute  
345 values of  $\delta^{18}\text{O}$  are close to the multiannual seasonal averages (Table 3). The highest decadal values of  $\delta^{18}\text{O}$  in both seasons  
346 are observed in 1912-1920. While a recent warming trend is observed in the regional meteorological data (in warm season),  
347 it is much less prominent in the ice core  $\delta^{18}\text{O}$  record, suggesting a divergence between  $\delta^{18}\text{O}$  and regional temperature. One of  
348 the possible explanations for this feature is the post-depositional change of the isotopic composition. But we do not expect a  
349 significant influence of the post-depositional processes because of high snow accumulation rate. The highest  $\delta^{18}\text{O}$  values for  
350 a single year correspond to the warm periods of 1984 and 1928, two years for which no unusual feature is identified from  
351 meteorological observations. The highest snow accumulation rate (fig. 9) is observed in both seasons of 2010, in coherence  
352 with the meteorological precipitation data, and also corresponding with a record low winter NAO index.  
353 Our deuterium excess record (fig. 2b) does not depict any robust seasonal variation. Moreover, the distribution of deuterium  
354 excess as a function of  $\delta^{18}\text{O}$  does not display any clear structure. By contrast, deuterium excess is weakly positively  
355 correlated with the accumulation rate during warm season ( $r = 0.31$ ,  $p < 0.05$ ). This finding is consistent with the GNIP data in  
356 the region that show no link between  $\delta^{18}\text{O}$  and deuterium excess. The smoothed values of deuterium excess have prominent  
357 cycles with a period of about 25 years that are synchronous in both seasons (fig. 6). Deuterium excess is highly sensitive to  
358 surface humidity, which itself is very different and depends on the arrival of maritime air masses or dry continental air  
359 masses. This may add to the complexity of the deuterium excess signal (Pfahl and Wernli, 2008).

### 361 **3.3 Comparison of ice core records with regional meteorological data**

362  
363 We compared the ice core data with the regional meteorological data and the large scale modes of variability. The result of  
364 the correlation analysis is summarized in Table 4. Multiannual variations of the parameters are shown in fig. 9 for the cold  
365 season and in fig. 10 for the warm season.

366 We found no significant correlation between the ice core  $\delta^{18}\text{O}$  record and regional temperature, neither with the reanalysis  
367 data, nor with the observation data, when using the whole period. A significant correlation ( $r = 0.44$ ,  $p < 0.05$ ) emerges for  
368 warm season data, when calculated for the period since 1984. The slope for this period is 0.6 per mille per °C. We also  
369 repeated our linear correlation analysis using precipitation weighted temperature, and obtained the same results. The  
370 precipitation weighted temperature was calculated using daily meteorological data. We used data from two stations:  
371 Klukhorskiy Pereval (as a representative of southern stations) and Mineralnye Vody (as a representative of the northern  
372 stations). We didn't find any statistically significant correlations when compared 3-, 5-, 7-years running means of these  
373 parameters. This result implies that the isotopic composition at Elbrus is controlled by both local and regional factors such as

374 changes in moisture sources. The possibilities for accurate reconstructions of past temperatures are therefore limited. For  
375 more accurate investigation of the  $\delta^{18}\text{O}$  – temperature relation on-site experiments and subsequent modeling is required. Our  
376 results are comparable to those obtained in the Alps by Mariani et al. (2014): again, while the seasonal cycle of ice core  $\delta^{18}\text{O}$   
377 appears related to that of temperature, this is not the case for inter-annual variations, driven by other factors such as changes  
378 in moisture sources. Another research performed in the Alps by Bohleber et al. (2013) revealed significant correlation of  
379 modified local temperature and the ice core isotopic composition at decadal scale. The authors also report that there are some  
380 periods of correlation absence. The main finding is that for the periods of less than 25 years the difference between the  
381 modified according to the authors' method and original dataset temperature is crucial but for longer periods the two  
382 temperature datasets are close to each other. That conclusion implies that the isotopic composition reflects the local  
383 temperature in the high mountain regions to a limited extent. It seems to be impossible to calculate the modified temperature  
384 for the Caucasus region according to the methods described by Bohleber et al. (2013) because of the relatively short and  
385 sparse original datasets.

386 Seasonal accumulation rate is linked to the precipitation rate on the stations situated south of the Caucasus in both seasons  
387 ( $r = 0.49$ ), and even more closely related to precipitation from Klukhorski Pereval station ( $r = 0.63$  for both seasons). We  
388 therefore establish a linear regression model for the period 1966-2013, and use this methodology to reconstruct past  
389 precipitation rates for the Klukhorskiy Pereval station (1914-1965), when meteorological records are not reliable or not  
390 available. The reconstructed records are shown on fig. 9 and 10 for the cold and warm seasons respectively. We found no  
391 significant trend in the reconstructed precipitation values. Even so, these results can be useful for validation of regional  
392 climate models and water resource assessment.

393 Calculation of the seasonal cycle of precipitation isotopic composition using the LMDZiso model (Risi et al., 2010) do not  
394 correspond to the results obtained from the ice core in absolute values or in amplitude (Fig. S5). This can be explained by a  
395 complicated relief of the region that influences strongly the isotopic composition, but it is not taken into account in the  
396 model. Also in summer Elbrus is in a local convective precipitation system that is not included in the model.

### 397 398 **3.4 Comparison of ice core records with large scale modes of variability**

399  
400 We didn't find any statistically significant correlations between ice cores data and large scale modes of variability when  
401 using the mean annual values. We present the results of calculations in the table 4. We report a weak though significant  
402 ( $p < 0.05$ ) negative correlation ( $r = -0.18$ ) between the ice core accumulation rate record and NAO in cold season. Moreover,  
403 the year of extremely high accumulation in both seasons (2010) coincides with an extremely low NAO winter index. The  
404 role of NAO in regional climate had also been evidenced by Shahgedanova et al. (2005) for the mass-balance of the  
405 Djankuat glacier situated in 30 km south-east of Elbrus for the period of 1967-2001. Interestingly, the accumulation record is  
406 related to the variability of regional precipitation, but the latter is not significantly related to the NAO. This may suggest  
407 different influences of large-scale atmospheric circulation on precipitation at lower versus higher elevations.

408 The ice core cold season  $\delta^{18}\text{O}$  record shows a positive correlation with the NAO index ( $r = 0.41$ ), while the NAO index is  
409 negatively correlated with regional temperature ( $r = -0.42$ ). It also contradicts the findings of Baldini et al (2008) who, based  
410 on the GNIP low elevation dataset, extrapolated a negative correlation between the  $\delta^{18}\text{O}$  of precipitation and the NAO in this  
411 region. This finding also suggests different drivers of temperature and  $\delta^{18}\text{O}$  at low and higher elevation. We propose the  
412 following explanation for this correlation. During the positive NAO phase, the predominant moisture source for the  
413 Caucasus precipitation is the Mediterranean. During the negative NAO phase the moisture source is the Atlantic. In the first  
414 case the precipitation  $\delta^{18}\text{O}$  preserved in the ice core is higher because of higher initial sea water isotopic composition (Gat et  
415 al., 1996) and shorter distillation pathway. It is also the continental recycling of moisture (Eltahir and Bras, 1996) that  
416 influences the water isotopic composition. Due to this process the  $\delta^{18}\text{O}$  values became lower while  $d$  values increase  
417 (Aemisegger et al., 2014) which is observed in our ice core data. In the opposite situation the initial water isotopic  
418 composition is close to 0 ‰ (Frew et al., 2000) and the distillation pathway is longer which leads to lower values of  
419 precipitation  $\delta^{18}\text{O}$ .

420 .  
421 We explored the links between the ice core parameters ( $\delta^{18}\text{O}$ , accumulation rate) with the NCP index and found no  
422 significant correlation neither in winter nor in summer despite the significant correlation between the NCP and local  
423 temperature and precipitation. A possible explanation may be that the NCP pattern only affects low elevation regional  
424 climate but not high elevation climate.

425 No significant correlation was identified between deuterium excess and indices of large scale modes of variability. So far, no  
426 regional or large-scale climate signal could be identified in Elbrus deuterium excess. Further investigations using  
427 backtrajectories and diagnoses of moisture source and evaporation characteristics will be needed to explore further the  
428 drivers of this second-order isotopic parameter.

#### 429 430 **4 Conclusion**

431  
432 We found no persistent link between ice cores  $\delta^{18}\text{O}$  and temperature on interannual scale, common feature emerging from  
433 non-polar ice cores (e.g. Mariani et al., 2014). This finding is not an artifact of high elevation versus low elevation difference  
434 because the variability of the regional temperature stack used for this comparison is in good agreement with the variability of  
435 the temperature at the drilling site as observed by the local AWS.

436 Our ice core records depict large decadal variations in  $\delta^{18}\text{O}$  with high and variable values in the late 19<sup>th</sup> - early 20<sup>th</sup>  
437 centuries, lower and more stable values in the 1940s-1960s, followed by a step increase in the 1970s. No unusual recent  
438 change is detected in the isotopic composition or in the accumulation rate record, in contrast with the observed warming  
439 trend from regional meteorological data. The accumulation rate appears significantly related to the NAO index coherently  
440 with the earlier results for the Djankuat glacier (Shahgedanova et al. 2005).

441 Based on regional meteorological information and trajectory analyses, the main moisture source is situated not far from the  
442 drilling site in warm season, and consists of evaporation from the Black Sea and continental evapotranspiration. Changes in  
443 regional temperature during warm season may affect the initial vapour isotopic composition as well as the atmospheric  
444 distillation processes, including convective activity, in a complex way. This may explain the significant albeit non persistent  
445 correlation of summer  $\delta^{18}\text{O}$  and temperature. Cold season moisture sources appear more variable geographically, with  
446 potential contributions from the North Atlantic to the Mediterranean regions. Changes in moisture origin appear to dominate  
447 in regional temperature-driven distillation processes. As a result, the ice core isotopic composition appears mostly related to  
448 characteristics of large –scale atmosphere circulation such as the NAO index. The changes in moisture origin also influence  
449 deuterium excess parameter, which does not have any prominent seasonal variations.

450 Our data can be used in atmospheric models equipped with water stable isotopes for instance in order to assess their ability  
451 to resolve NAO – water isotope relationships (Langebroek et al., 2011, Casado et al., 2014). The accumulation rate at the  
452 drilling site is significantly correlated with the precipitation rate and gives information about precipitation variability before  
453 the beginning of meteorological observations.

#### 455 **Acknowledgements**

456  
457 The research was supported by the RFBR grant 14-05-31102. The analytical procedure ensuring a high accuracy of isotope  
458 data obtained at CERL was elaborated with financial support from the Russian Science Foundation, grant 14-27-00030. The  
459 study of dust layers was conducted with the support of RFBR grant 14-05-00137. The measurement of the samples in IAEA  
460 was conducted according to research contracts 16184\R0, and 16795. This research work was conducted in the framework of  
461 the International Associated Laboratory (LIA) “Climate and Environments from Ice Archives” 2012–2016, linking several  
462 Russian and French laboratories and institutes. We thank Obbe Tuinenburg and Jean-Louis Bonne for the back trajectories  
463 calculations.

#### 465 **References**

- 466 Aemisegger F., Pfahl S., Sodemann H., Lehner I., Seneviratne S.I., Wernli H.: Deuterium excess as a proxy for continental  
467 moisture recycling and plant transpiration, *Atmos. Chem. Phys*, 14, 4029–4054, doi:10.5194/acp-14-4029-2014, 2014.
- 468 Baldini L.M., McDermott F., Foley A.M., Baldini J.U.L.: Spatial variability in the European winter precipitation  $\delta^{18}\text{O}$ -NAO  
469 relationship: Implications for reconstructing NAO-mode climate variability in the Holocene, *Geophys. Res. Letters*. 35,  
470 doi:10.1029/2007GL032027, L04709, 2008.
- 471 Bohleber P., Wagenbach D., Schonher W., Bohm R.: To what extent do water isotope record from low accumulation Alpine  
472 ice cores reproduce instrumental temperature series? *Tellus B*, 65, 20148, doi:10.3402/tellusb.v65i0.20148, 2013.
- 473 Brunetti M., Kutiel H.: The relevance of the North-Sea Caspian Pattern (NCP) in explaining temperature variability in  
474 Europe and the Mediterranean, *Nat. Hazards Earth Syst. Sci.*, 11, 2881–2888, doi:10.5194/nhess-11-2881-2011, 2011.

475 Casado M, Ortega P., Masson-Delmotte V., Risi C., Swingedouw D., Daux V., Genty D., Maignan F., Solomina O., Vinter  
476 B., Viovy N., Yiou P.: Impact of precipitation intermittency on NAO-temperature records, *Clim. Past*, 9, 871-886,  
477 doi:10.5194/cp-9-871-2013, 2013.

478 Comas-Bru, L., McDermott, F. and Werner, M. (2016): The effect of the East Atlantic pattern on the precipitation  $\delta^{18}\text{O}$ -  
479 NAO relationship in Europe, *Climate Dynamics*, doi: 10.1007/s00382-015-2950-1

480 Dansgaard, W.: Stable isotopes in precipitation, *Tellus*, 16(4), 436-468, 1964

481 Dansgaard, W., Johnsen, S.J.: A flow model and a time scale for the ice core from Camp Century, Greenland, *J. Glaciol.*,  
482 8(53), 215-223, 1969.

483 Draxler, R.R., and Hess G.D.: An overview of the HYSPLIT\_4 modeling system of trajectories, dispersion, and deposition.  
484 *Aust. Meteor. Mag.*, 47, 295-308, 1998.

485 Ekaykin A.A., Lipenkov V.Ya.: Formation of the ice core isotopic composition, *Physics of ice core records II*, ed. T.Hondoh,  
486 *Low Temperature Science*, 68, Hokkaido Univ. Press, Sapporo, 299-314, 2009.

487 Elizbarashvili E.Sh., Elizbarashvili, M.R., Tatishvili, M.E., Elizbarashvili, Sh.E., Elizbarashvili, R.Sh.: Meskhiya Air  
488 temperature trends in Georgia under global warming conditions, *Russ. Meteorol. Hydrol.*, 38, 234-238, 2013.

489 Eltahir E.A.B., Bras R.L.: Precipitation recycling, *Reviews of Geophysics* 34, 3, 367-378, doi: 8755-12 09/96/96 RG-01927,  
490 1996

491 Forster C., Stohl A., Siebert P.: Parametrization of convective transport in a lagrangian particle dispersion model and its  
492 evaluation, *Journ. of Applied Meteorology and Climatology*, 46 (4), 403-422, doi:10.1175/JAM2470.1, 2007.

493 Frew, R., Dennis, P.F., Heywood K.J., Meredith M.P., and Boswell S.M.: The oxygen isotope composition of water masses  
494 in the northern North Atlantic, *Deep Sea Research Part I: Oceanographic Research Papers*, 47, 12, 2265-2286,  
495 doi:10.1016/S0967-0637(00)00023-6, 2000.

496 Gat, J.R., Shemesh, A., Tziperman, E., Hecht, A., Georgopoulos, D., and Basturk, O.: The stable isotope composition of  
497 waters of the eastern Mediterranean Sea, *J. Geophysical Res.*, 101, 3, 6441-6451, doi: 10.1029/95JC02829, 1996.

498 Johnsen S., Clausen H.B., Cuffey K.M., Hoffmann G., Schwander J., Creyts T.: Diffusion of stable isotopes in polar firn and  
499 ice: the isotope effect in firn diffusion, *Physics of Ice Core Records*, Edited by T. Hondoh, Hokkaido University Press,  
500 Sapporo, 121-140, 2000.

501 Kalnay, E., Kanamitsu, M., Kistler, R., Collins, W., Deaven, D., Gandin, L., Iredell, M., Saha, S., White, G., Woollen, J.,  
502 Zhu, Y., Leetmaa, A., Reynolds, B., Chelliah, M., Ebisuzaki, W., Higgins, W., Janowiak, J., Mo, K. C., Ropelewski, C.,  
503 Wang, J., Jenne, R., Joseph, D.: The NCEP/NCAR 40-Year Reanalysis Project, *Bulletin of the American Meteorological*  
504 *Society*, 77, 3, 437-472, doi: 10.1175/1520-0477(1996)077<0437:TNYRP>2.0.CO;2, 1996.

505 Kozachek A.V., Ekaykin A.A., Mikhaleiko V.N., Lipenkov V.Y., Kutuzov S.S.: Isotopic composition of ice cores obtained  
506 at the Elbrus Western Plateau, *Ice and Snow*, 55, 4, doi: 10.15356/2076-6734-2015-4-35-49, 35-49, 2015 (in Russian with  
507 English summary)

508 Kutuzov, S., Shahgedanova, M., Mikhaleiko, V., Lavrentiev, I., and Kemp, S.: Desert dust deposition on Mt. Elbrus,  
509 Caucasus Mountains, Russia in 2009–2012 as recorded in snow and shallow ice core: high-resolution “provenancing”,  
510 transport patterns, physical properties and soluble ionic composition, *The Cryosphere*, 7(5), 1481–1498, doi:10.5194/tc-7-  
511 1481-2013, 2013.

512 Langebroek, P. M.; Werner, M.; Lohmann, G.: Climate information imprinted in oxygen-isotopic composition of  
513 precipitation in Europe, *Earth and Planetary Science Letters*, 311, 1, 144-154, 10.1016/j.epsl.2011.08.049, 2011.

514 Mariani I., Eichler A., Jenk M., Brönnimann S., Auchmann R., Leuenberger M.C., Schwikowski M.: Temperature and  
515 precipitation signal in two Alpine ice cores over the period 1961–2001, *Clim. Past.* 10, 1093–1108, doi:10.5194/cp-10-1093-  
516 2014, 2014.

517 Mikhaleiko V., Sokratov S., Kutuzov S., Ginot P., Legrand M., Preunkert S., Lavrentiev I., Kozachek A., Ekaykin A., Faïn  
518 X., Lim S., Schotterer U., Lipenkov V., Toropov P.: Investigation of a deep ice core from the Elbrus western plateau, the  
519 Caucasus, Russia, *The Cryosphere*, 9, 2253-2270, doi:10.5194/tc-9-2253-2015, 2015.

520 Mikhaleiko, V.N., Kuruzov, S.S., Lavrentiev, I.I., Kunakhovich, M.G., and Thompson, L.G.: Issledovanie zapadnogo  
521 lednikovogo plato Elbrusa: rezul'taty i perspektivy (Western Elbrus Plateau studies: results and perspectives), *Materialy*  
522 *glyatsiologicheskikh issledovaniy (Data Glaciol. Stud.)*, (99), 185–190, 2005 (in Russian with English summary)

523 Mountain Research Initiative EDW Working Group: Elevation-dependent warming in mountain regions of the world, *Nature*  
524 *Climate Change* 5, 424–430, doi:10.1038/nclimate2563, 2015.

525 Panagiotopoulos F., Shahgedanova M., Steffenson D.B.: A  
526 review of Northern Hemisphere winter time teleconnection patterns, *J. Phys. IV France*, 12, doi: 10.1051/jp4:20020450,  
2002.

527 Persson, A., P. L. Langen, P. Ditlevsen, B. M. Vinther: The influence of precipitation weighting on interannual variability of  
528 stable water isotopes in Greenland, *J. Geophys. Res.*, 116, D20120, doi:10.1029/2010JD015517, 2011.

529 Pfahl S. and Wernli H.: Air parcel trajectory analysis of stable isotopes in water vapor in the eastern Mediterranean, *J.*  
530 *Geophys. Res.*, 113, D20104, doi:10.1029/2008JD009839, 2008.

531 Risi C., Bony S., Vimeux F., Jouzel J.: Water stable isotopes in the LMDZ4 general circulation model: Model evaluation for  
532 present-day and past climate and implications to climatic interpretation of tropical isotopic records, *Journal of Geophysical*  
533 *Research*, 115, D12118, doi:10.1029/2009JD013255, 2010.

534 Rolph, G.D., Real-time Environmental Applications and Display sYstem (READY) Website (<http://ready.arl.noaa.gov>).  
535 NOAA Air Resources Laboratory, Silver Spring, MD, 2016.

536 Shahgedanova M., Nosenko G., Kutuzov S., Rototaeva O., and Khromova T.: Deglaciation of the Caucasus Mountains,  
537 Russia/Georgia, in the 21st century observed with ASTER satellite imagery and aerial photography, *The Cryosphere*, 8(6),  
538 2367–2379, doi:10.5194/tc-8-2367-2014, 2014.

539 Shahgedanova M., Stokes C., Gurney S., Popovnin V.: Interactions between mass balance, atmospheric circulation, and  
540 recent climate change on the Djankuat Glacier, Caucasus Mountains, Russia, *Journ. of Geophys. Research*, 110, D04108,  
541 doi:10.1029/2004JD005213, 2005.



542 Stein, A.F., Draxler, R.R, Rolph, G.D., Stunder, B.J.B., Cohen, M.D., and Ngan, F.: NOAA's HYSPLIT atmospheric  
543 transport and dispersion modeling system, *Bull. Amer. Meteor. Soc.*, 96, 2059-2077, doi: 10.1175/BAMS-D-14-00110.1,  
544 2015.

545 Stoffel M., Khodri M., Corona C., Guillet S., Poulain V., Bekki S., Guiot J., Luckman B.H., Oppenheimer C., Lebas N.,  
546 Beniston M., and Masson-Delmotte V.: Estimates of volcanic-induced cooling in the Northern Hemisphere over the past  
547 1,500 years, *Nature Geoscience* 8, 784–788, doi:10.1038/ngeo2526, 2015.

548 Stohl A., Thompson D.J.: A density correction for lagrangian particle dispersion models, *Boundary Layer Meteorology*, 90  
549 (1), 155–167, doi:10.1023/A:1001741110696, 1999.

550 Tielidze L.G.: Glacier change over the last century, Caucasus Mountains, Georgia, observed from old topographical maps,  
551 Landsat and ASTER satellite imagery, *The Cryosphere*, 10, 713-725, doi:10.5194/tc-10-713-2016, 2016.

552 Toropov P.A., Mikhailenko V.N., Kutuzov S.S., Morozova P.A., Shestakova A.A.: Temperature and radiation regime of  
553 glaciers on slopes of the Mount Elbrus in the ablation period over last 65 years, *Ice and Snow*, 56(1), 5-19,  
554 doi:10.15356/2076-6734-2016-1-5-19, 2016 (In Russian with English summary).

555 Tsushima A., Matoba S., Shiraiwa T., Okamoto S., Sasaki H., Solie D.J., Yoshikawa K.: Reconstruction of recent climate  
556 change in Alaska from the Aurora Peak ice core, central Alaska, *Clim. Past*, 11, 217–226, doi:10.5194/cp-11-217-2015,  
557 2015.

558 Vinther, B. M., S. J. Johnsen, K. K. Andersen, H. B. Clausen, A. W. Hansen: NAO signal recorded in the stable isotopes of  
559 Greenland ice cores, *Geophys. Res. Lett.*, 30(7), 1387, doi:10.1029/2002GL016193, 2003

560 Vinther B.M., Jones P.D., Briffa K.B., Clausen H.B., Andersen K.K., Dahl-Jensen D., Johnsen S.J.: Climatic signals in  
561 multiple highly resolved stable isotopes records from Greenland, *Quat. Sci. Rev.* 29 (3-4), 522-538, 2010

562 Volodicheva, N.: The Caucasus, in: *The Physical geography of Northern Eurasia*, edited by: Shahgedanova, M., Oxford  
563 University Press, Oxford, 350–376, 2002

564 .

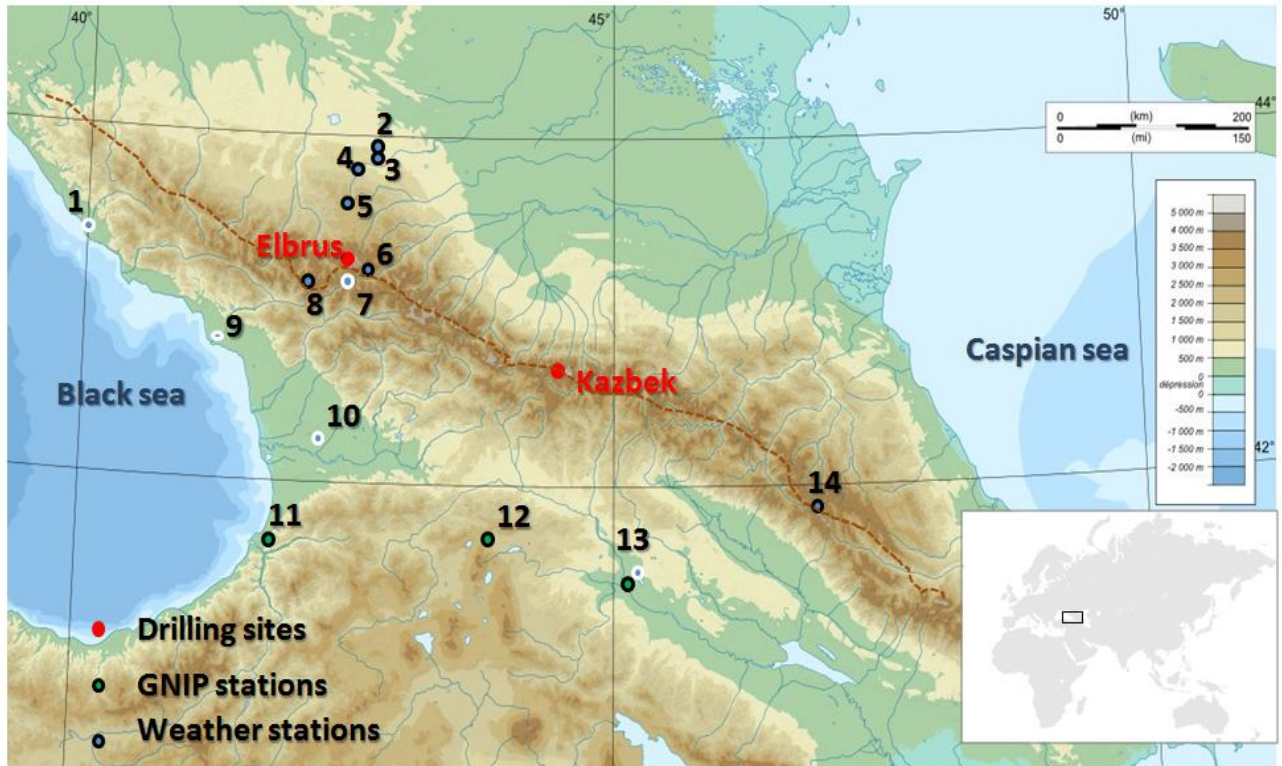
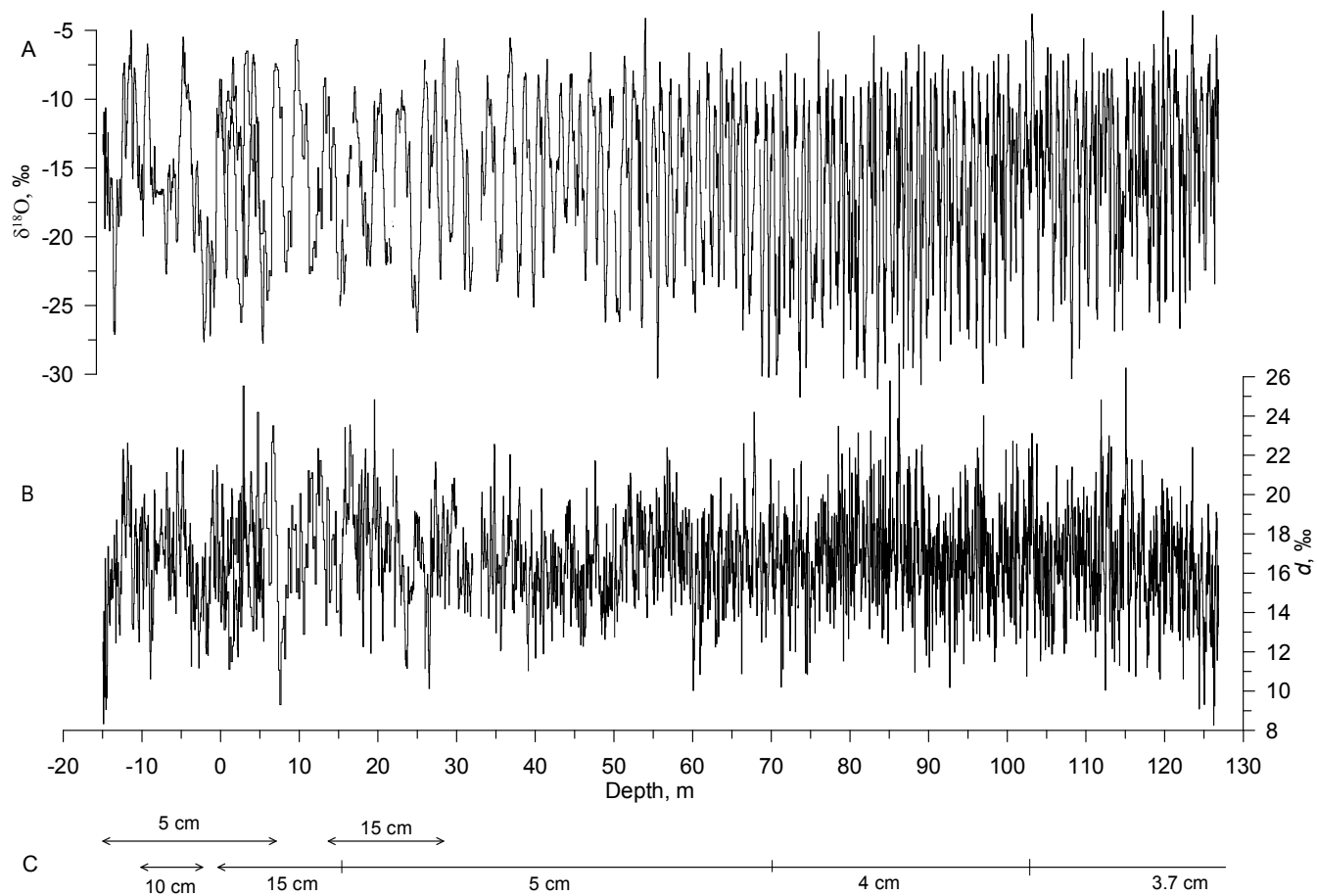
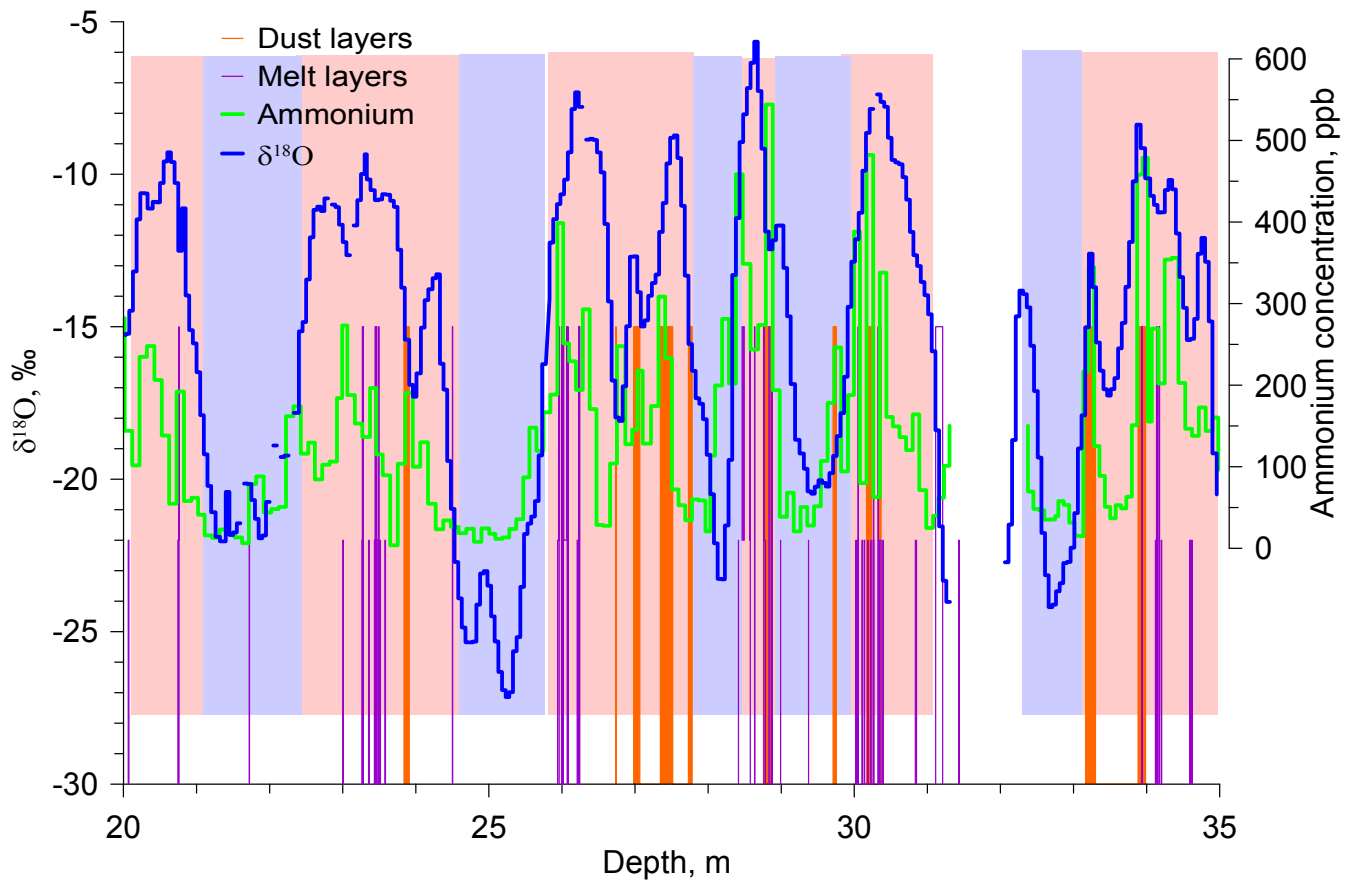


Fig. 1: Map showing the region around Elbrus (black rectangle in the world's map in the lower right corner), with shading indicating elevation (m above sea level). Drilling sites are indicated with red filled circles, GNIP stations as green filled circles, and meteorological stations as blue dots. Stations situated to the south of the Main Caucasus Ridge according to the precipitation cycle pattern are shown using a blue dot with white outside circle and the stations situated to the north are displayed with black outside circle (see text for the details). The brown dotted line shows the border between two types of precipitation seasonal cycles. The number of the various stations refers to Table 1 for their detailed description.



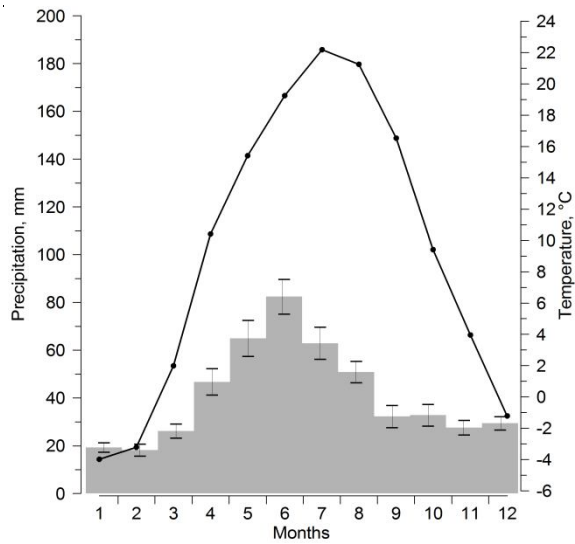
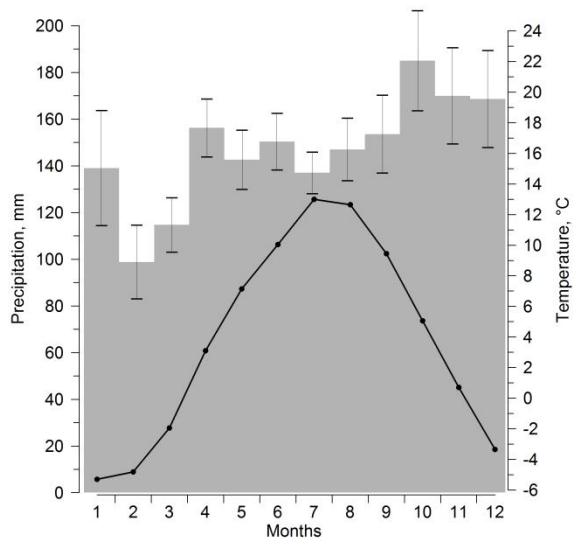
577  
578  
579  
580  
581

**Fig. 2. Vertical profile of  $\delta^{18}\text{O}$  (A), deuterium excess (B), and the number of the ice core as well as sampling resolution (C). 0 m depth corresponds to the surface of 2009.**

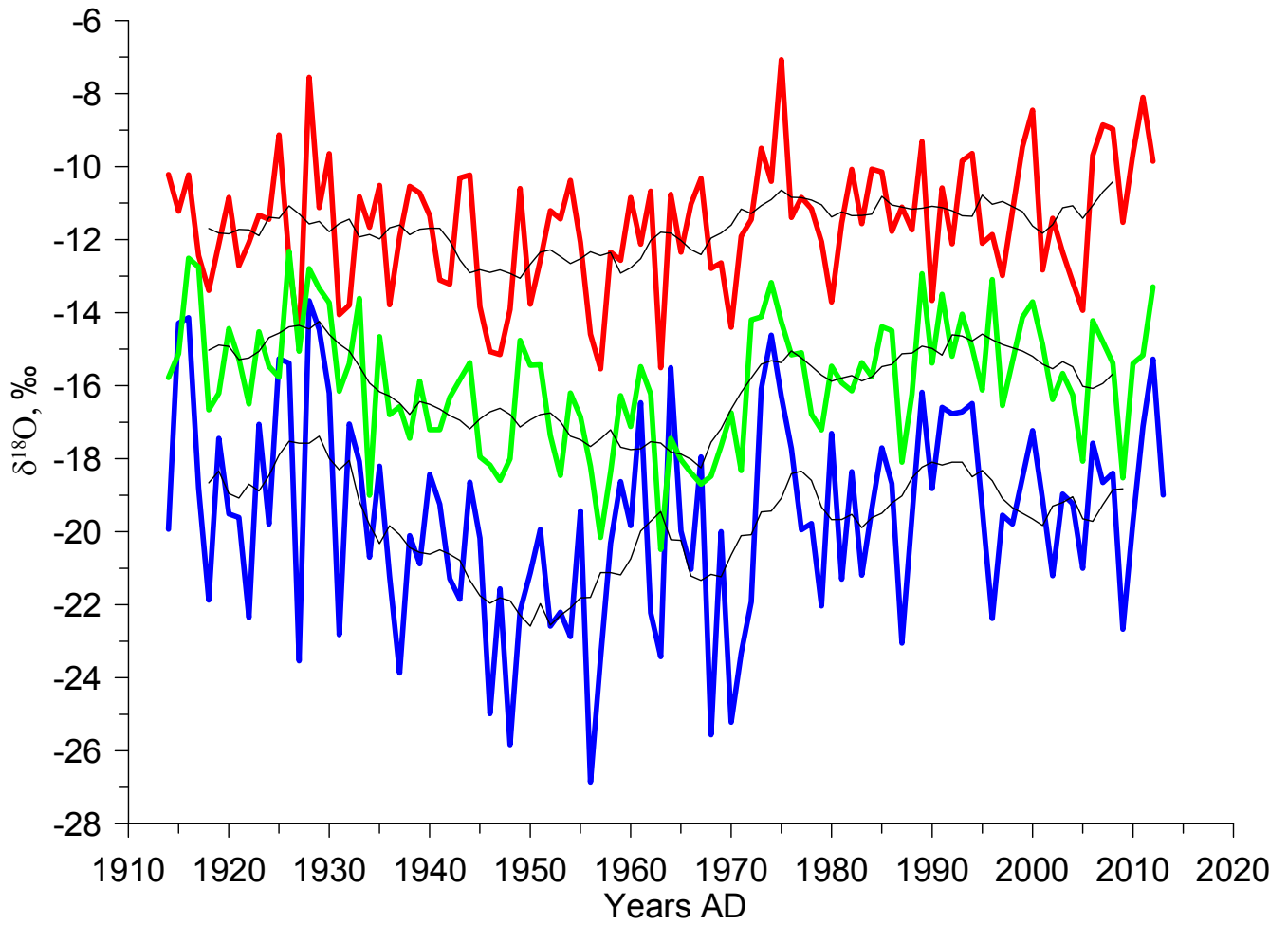


582  
 583  
 584  
 585  
 586  
 587

Fig. 3: Illustration of the scheme used to identify warm and cold half-years (respectively indicated by the light red and light blue shaded areas) based on the deviation of the mean  $\delta^{18}\text{O}$  values from the long-term average value. The purple lines depict the melt layers observed in the core, dust layers are shown in orange and ammonium concentration graph (Mikhaleiko et al., 2015) is in green.

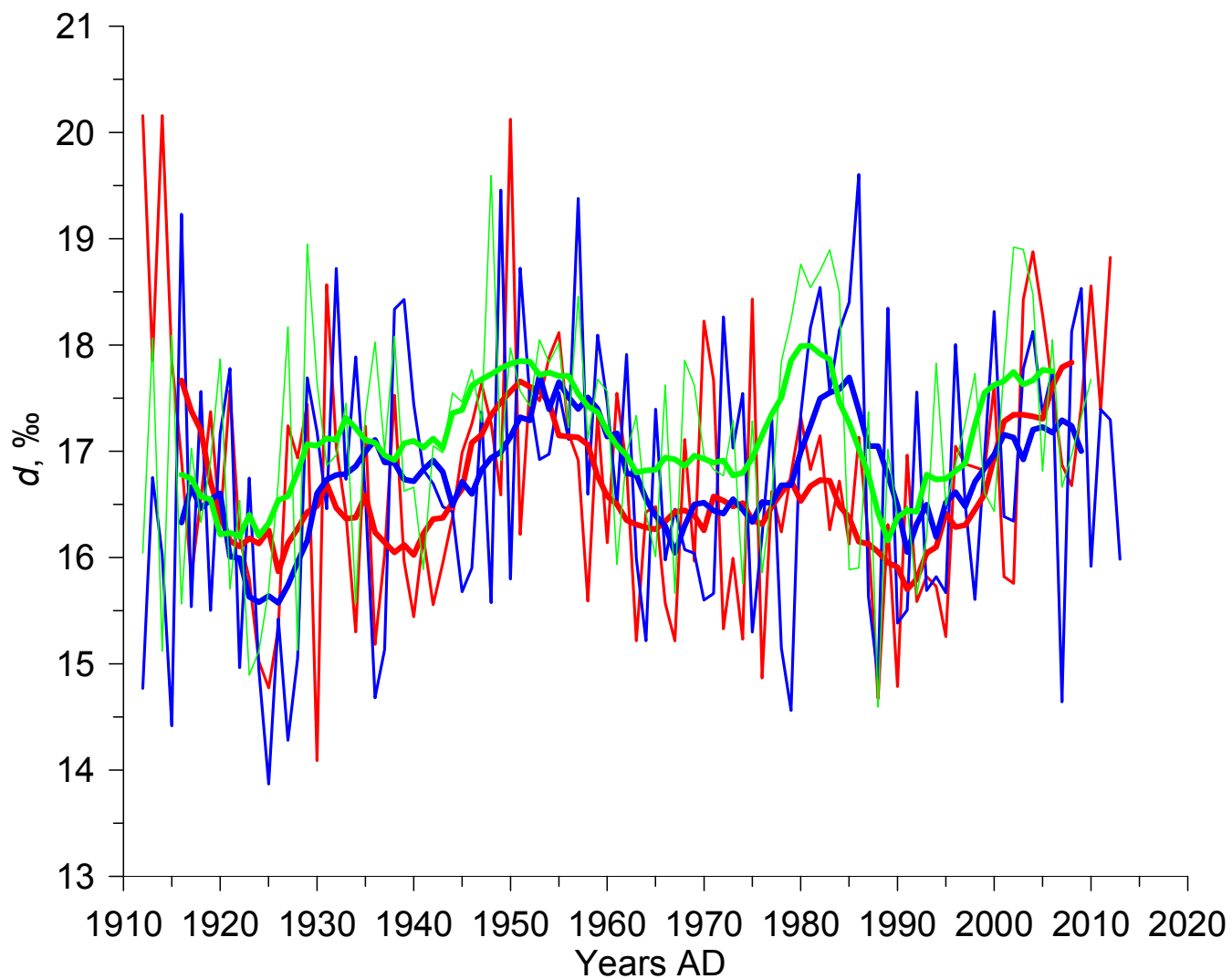


588  
 589  
 590 **Fig. 4: Average seasonal cycle of temperature (black dots and line) and precipitation (grey bars) calculated over 1966-1990 period,**  
 591 **a) for the Klukhorskyy Pereval station (illustrating the lack of a distinct seasonal cycle in precipitation south of the Caucasus) and**  
 592 **b) for the Mineralnye Vody station (illustrating the clear seasonal cycle in precipitation seen in stations north of the Caucasus).**  
 593 **Error bars (SEM) are shown for the interannual standard deviation of the monthly precipitation rate while the same error bars**  
 594 **for the temperature are dimensionless at the scale of the graph.**  
 595



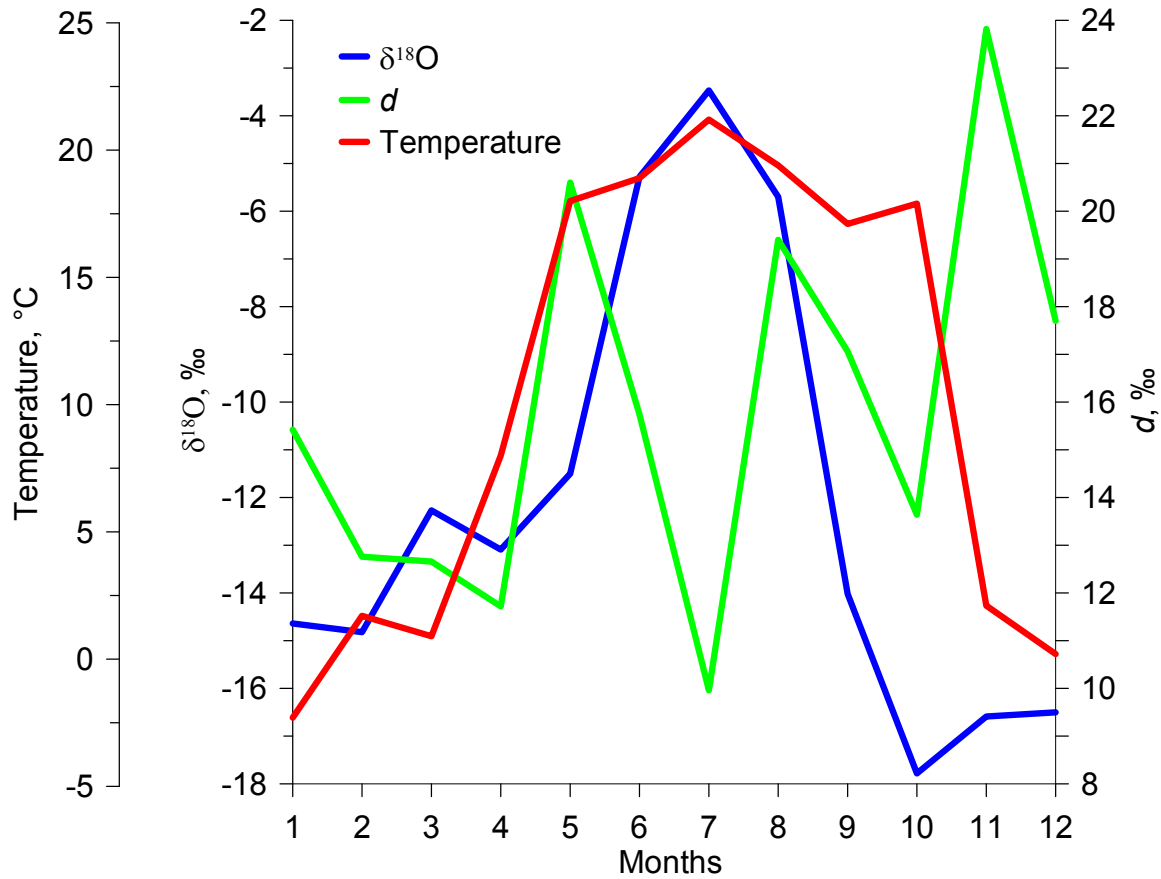
596  
597  
598  
599

Fig. 5: Annual variations of  $\delta^{18}\text{O}$  in warm season (red line), in cold season (blue line), and annual means (green line). Thin black lines show 10-year running means of these parameters.



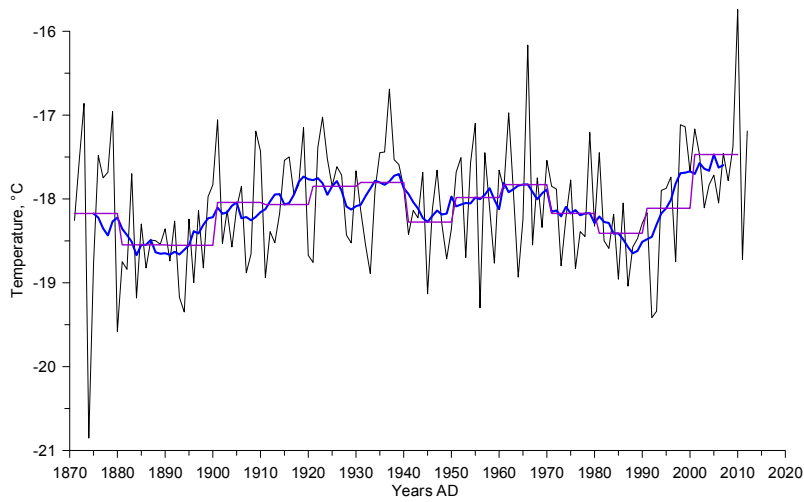
600  
601  
602  
603

Fig. 6: Annual variations of deuterium excess in warm season (red line), in cold season (blue line), and mean annual values (green line). Thick lines show the 10-year smoothed values and the thin ones display the raw values.

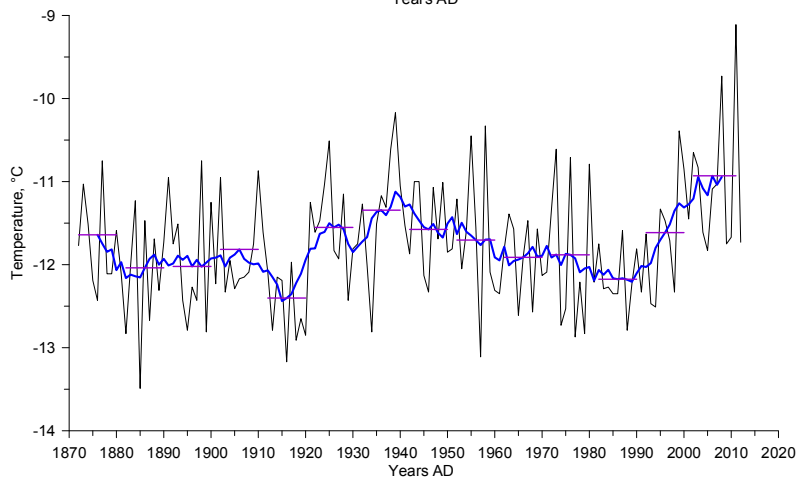


605  
 606 Fig. 7: Monthly  $\delta^{18}\text{O}$  (blue line),  $d$  (green line) and air temperature (red line) data at Bakuriani GNIP station in 2009 (see Table 1  
 607 for information on station and Fig. 1 for its location). Note that there is no clear seasonal cycle in deuterium excess, in contrast  
 608 with  $\delta^{18}\text{O}$  showing maximum values in summer and minimum values in winter.  
 609

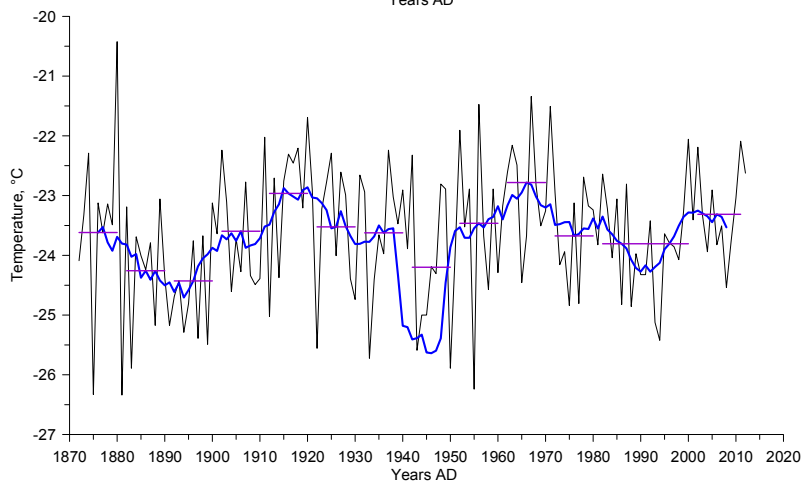




610



611



612

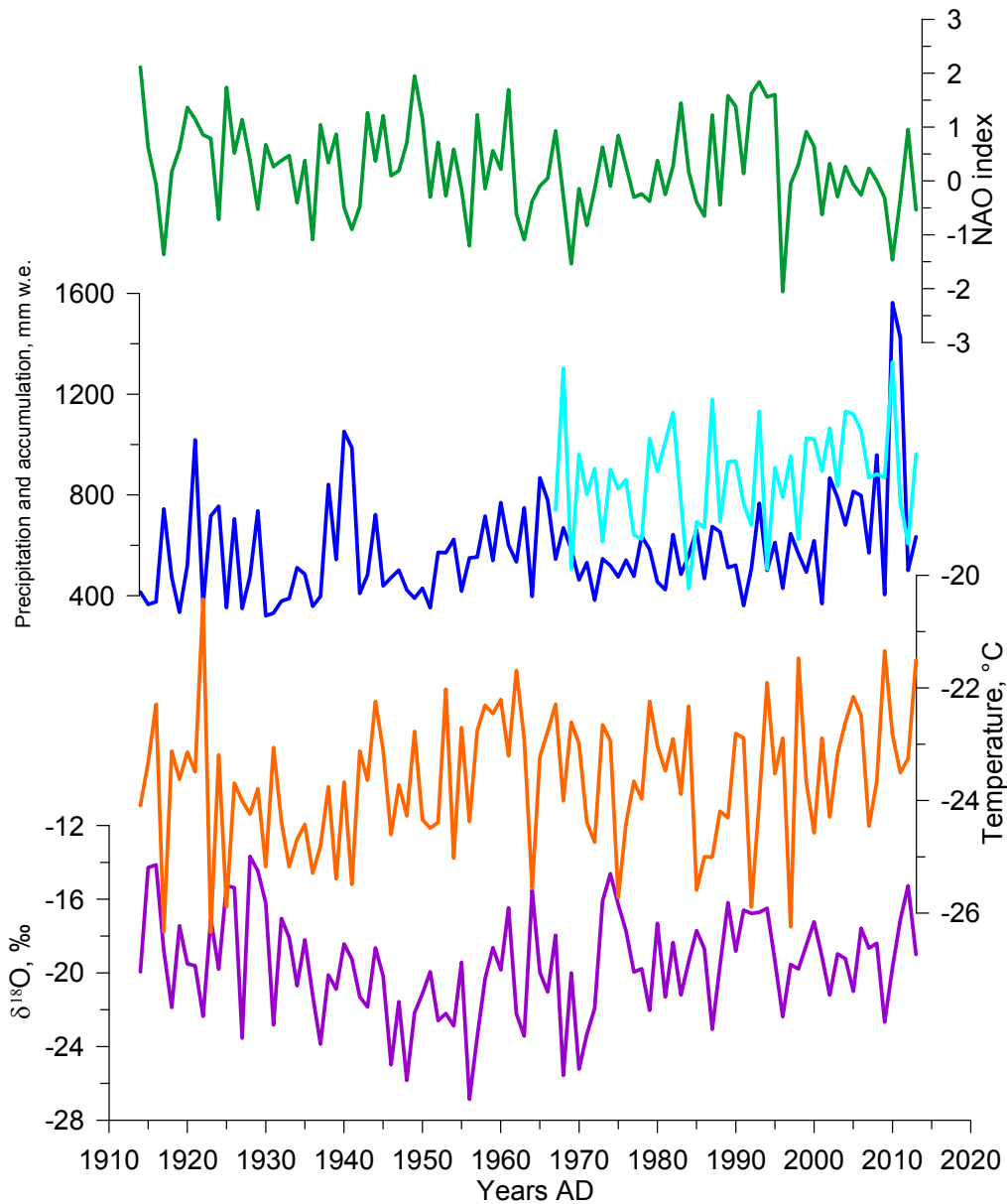
613

614

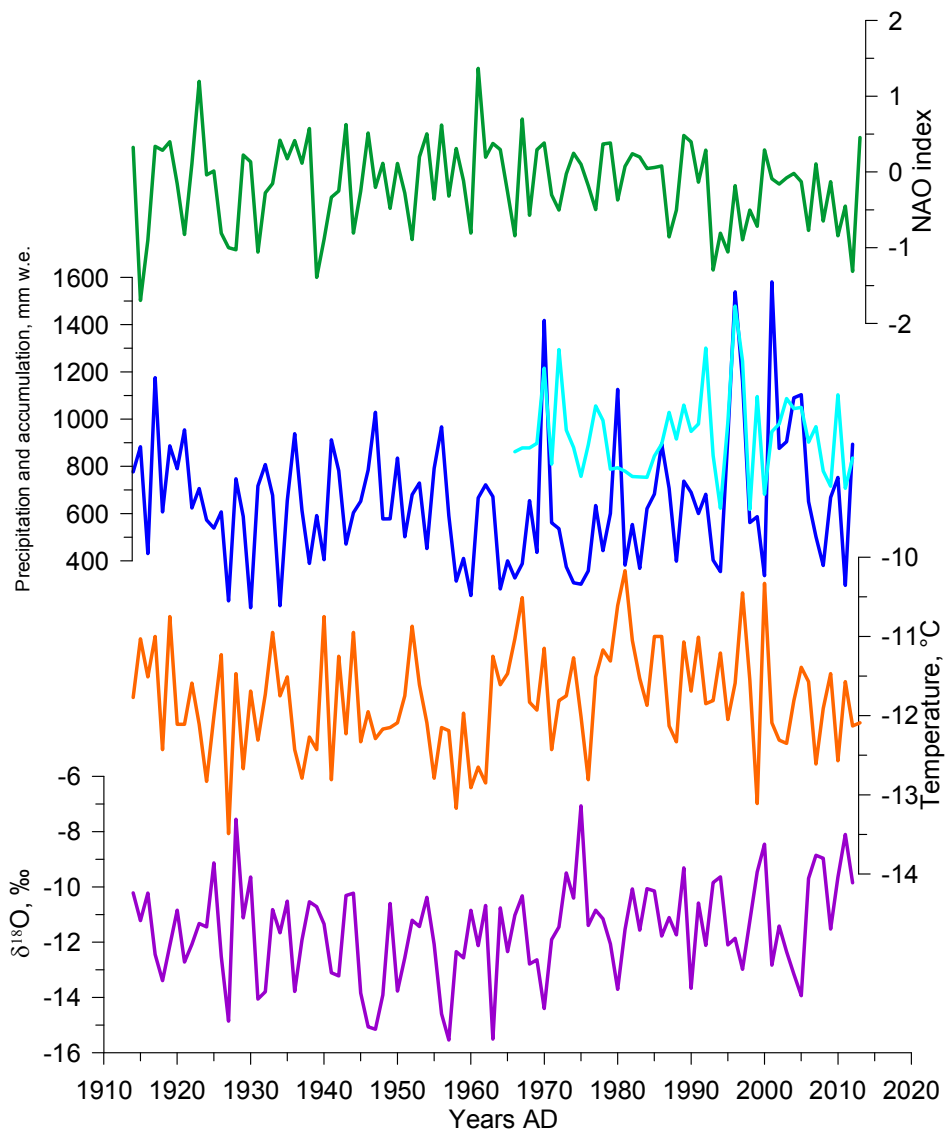
615

616

**Fig. 8: Normalized regional temperature record based on meteorological data, with respect to the reference period 1966-1990, expressed as annual anomalies (°C). The thin lines illustrate the standard deviation across the individual records after accounting for the lapse rate from Fig. S3, the blue line shows 10 year running mean and the horizontal purple line demonstrates the decadal mean value, the upper panel for the annual means, middle panel for the warm season, and the lower panel for the cold season.**



617  
 618 **Fig. 9: Comparison of the ice core record with instrumental regional climate information, for the cold season:  $\delta^{18}\text{O}$  composite**  
 619 **(purple), temperature at the drilling site calculated from the lapse rate (brown), precipitation at the Klukhorskii Pereval station**  
 620 **(light blue) as well as the ice core accumulation estimate (dark blue) and NAO index(green).**  
 621  
 622



623  
624  
625  
626

**Fig. 10:** Same as fig. 9 but for the warm season.

627  
628  
629  
630

631 **Table 1: Description of meteorological and instrumental data used in the paper**

Data type	Number on map (Fig. 1)	Location/Name	Altitude a.s.l.	Time span	Data source		
Meteorological observations (temperature, precipitation rate) with daily resolution	1	Sochi	57 m	1871-present	www.meteo.ru		
	2	Mineralnye Vody	315 m	1938-present			
	3	Kislovodsk	943 m	1940-present			
	4	Pyatigorsk	538 m	1891-1997			
	5	Shadzhatmaz	2070 m	1959-present			
	6	Terskol	2133 m	1951-2005			
	7	Klukhorskiy Pereval	2037 m	1959-present			
	8	Teberda	1550 m	1956-2005			
	9	Sukhumi	75 m	1904-1988			
	10	Samtredia	24 m	1936-1992			
	13	Tbilisi	448 m	1881-1992			
	14	Sulak	2927 m	1930-present			
	15	Mestia	1417 m	1930-1991			
	GNIP data	11	Batumi	32 m		1980-1990	<a href="http://www-naweb.iaea.org/napc/ih/IHS_resources_gnip.html">http://www-naweb.iaea.org/napc/ih/IHS_resources_gnip.html</a>
		12	Bakuriani	1700 m		2008-2009	
13		Tbilisi	448 m	2008-2009			
Circulation indices	n/a	NAO	n/a	1821-present	Vinter et al., 2009 <a href="https://crudata.uea.ac.uk/~timo/datasets/naoi.htm">https://crudata.uea.ac.uk/~timo/datasets/naoi.htm</a> <a href="http://www.cpc.ncep.noaa.gov/products/precip/CWlink/">http://www.cpc.ncep.noaa.gov/products/precip/CWlink/</a>		
			n/a	1950-present			
	n/a	NCP	n/a	1948-present			
	n/a	AO	n/a	1950-present			
Reanalysis daily temperature	n/a	NCEP	500 mb level	1948-present	<a href="http://www.esrl.noaa.gov/psd/data/gridded/data.ncep.reanalysis.html">http://www.esrl.noaa.gov/psd/data/gridded/data.ncep.reanalysis.html</a> Kalnay et al., 1996		
Back trajectories	n/a	Flexpart	n/a	2002-2009	Forster et al., 2007, Stohl et al., 2009		
	n/a	Hysplit	n/a	1948-present	Draxler, 1999, Stein et al., 2015, Rolph, 2016		
	n/a	LMDZiso	n/a	n/a	Risi et al., 2010		

632

633  
634  
635  
636  
637

**Table 2: Correlation coefficients between meteorological data and indices of large-scale modes of variability (statistically significant coefficients at  $p < 0.05$  are highlighted in bold). The period of calculation and number of data points (n) for each coefficient are shown in brackets.**

Annual mean	Temperature	P south*	P north*
NAO	<b>-0.24</b> (1914-2013, n=100)	-0.24 (1966-2013, n=48)	-0.03 (1966-2013, n=48)
AO	<b>-0.34</b> (1950-2013, n=64)	-0.06 (1966-2013, n=48)	0.02 (1966-2013, n=48)
NCP	<b>-0.55</b> (1948-2013, n=66)	0.26 (1966-2013, n=48)	0.26 (1966-2013, n=48)
Warm season			
NAO	<b>-0.47</b> (1914-2013, n=100)	0.23 (1966-2013, n=48)	0.03 (1966-2013, n=48)
AO	-0.11 (1950-2013, n=64)	0.08 (1966-2013, n=48)	0.14 (1966-2013, n=48)
NCP	<b>-0.50</b> (1948-2013, n=66)	<b>0.34</b> (1966-2013, n=48)	<b>0.34</b> (1966-2013, n=48)
Cold season			
NAO	<b>-0.41</b> (1914-2013, n=100)	0.04 (1966-2013, n=48)	0.26 (1966-2013, n=48)
AO	<b>-0.40</b> (1950-2013, n=64)	0.14 (1966-2013, n=48)	<b>0.37</b> (1966-2013, n=48)
NCP	<b>-0.77</b> (1948-2013, n=66)	0.25 (1966-2013, n=48)	<b>0.33</b> (1966-2013, n=48)

638  
639  
640  
641  
642  
643  
644

\*P south – precipitation rate at the weather stations to the South from the Caucasus, P north – precipitation rate at the weather stations to the North from the Caucasus.

645

**Table 3: Mean characteristics of the Elbrus ice core records, calculated for the period from 1914 to 2013.**

<b>Annual means</b>	$\delta^{18}\text{O}$ , ‰	$\delta\text{D}$ , ‰	$d$ , ‰	Accumulation rate (m w.e./year)
Mean	-15.90	-110.10	17.11	1,29
Standard deviation	1.76	14.03	1.02	0.44
<b>Cold season</b>				
Mean	-19.61	--140.11	16.59	0.71
Standard deviation	2.81	22.54	2.11	0.36
<b>Warm season</b>				
Mean	-11.58	-75.97	16.69	0.65
Standard deviation	1.75	13.98	1.14	0.27

646  
647

**Table 4. Correlation coefficients between ice core data, meteorological data and indices of large-scale modes of variability (statistically significant coefficients at  $p < 0.05$  are highlighted in bold). The period of calculation and number of data points (n) for each coefficient is shown in brackets.**

Annual means	$\delta^{18}\text{O}$	Accumulation	$d$	NAO	AO	NCP
$T. \text{ } ^\circ\text{C}$	-0.01 (1914-2013, n=100)	0.16 (1914-2013, n=100)	0.00 (1914-2013, n=100)	<b>-0.24</b> (1914-2013, n=100)	<b>-0.34</b> (1950-2013, n=64)	<b>-0.55</b> (1948-2013, n=66)
P north*	-0.30 (1966-2013, n=48)	0.36 (1966-2013, n=48)	0.17 (1966-2013, n=48)	-0.03 (1966-2013, n=48)	-0.03 (1966-2013, n=48)	<b>0.27</b> (1966-2013, n=48)
P south*	0.06 (1966-2013, n=48)	<b>0.52</b> (1966-2013, n=48)	0.07 (1966-2013, n=48)	-0.24 (1966-2013, n=48)	-0.06 (1966-2013, n=48)	<b>0.18</b> (1966-2013, n=48)
$\delta^{18}\text{O}$		-0.20 (1914-2013, n=100)	-0.06 (1914-2013, n=100)	0.07 (1914-2013, n=100)	<b>0.41</b> (1950-2013, n=64)	0.11 (1948-2013, n=66)
Accumulation			0.21 06 (1914-2013, n=100)	<b>-0.29</b> (1914-2013, n=100)	<b>-0.29</b> (1950-2013, n=64)	-0.03 (1948-2013, n=66)
$d$				-0.08 (1914-2013, n=100)	-0.26 (1950-2013, n=64)	-0.14 (1948-2013, n=66)
Warm season	$\delta^{18}\text{O}$	Accumulation	$d$	NAO	AO	NCP
$T. \text{ } ^\circ\text{C}$	0.13 (1914-2013, n=100)	-0.04 (1914-2013, n=100)	<b>0.20</b> (1914-2013, n=100)	-0.02 (1914-2013, n=100)	-0.10 (1950-2013, n=64)	<b>-0.51</b> (1948-2013, n=66)
P north*	0.01 (1966-2013, n=48)	0.16 (1966-2013, n=48)	0.09 (1966-2013, n=48)	0.13 (1966-2013, n=48)	-0.14 (1966-2013, n=48)	0.18 (1966-2013, n=48)
P south*	-0.27 (1966-2013, n=48)	<b>0.49</b> (1966-2013, n=48)	-0.02 (1966-2013, n=48)	-0.01 (1966-2013, n=48)	0.07 (1966-2013, n=48)	<b>0.34</b> (1966-2013, n=48)
$\delta^{18}\text{O}$		<b>-0.42</b> (1914-2013, n=100)	-0.05 (1914-2013, n=100)	-0.08 (1914-2013, n=100)	0.16 (1950-2013, n=64)	0.00 (1948-2013, n=66)
Accumulation			0.31 06 (1914-2013, n=100)	0.00 (1914-2013, n=100)	0.09 (1950-2013, n=64)	0.00 (1948-2013, n=66)
$d$				0.00 (1914-2013, n=100)	-0.01 (1950-2013, n=64)	-0.14 (1948-2013, n=66)
Cold season	$\delta^{18}\text{O}$	Accumulation	$d$	NAO	AO	NCP
$T. \text{ } ^\circ\text{C}$	-0.09 (1914-2013, n=100)	0.11 (1914-2013, n=100)	-0.15 (1914-2013, n=100)	<b>-0.30</b> (1914-2013, n=100)	<b>-0.45</b> (1950-2013, n=64)	<b>-0.79</b> (1948-2013, n=66)
P north*	0.20 (1966-2013, n=48)	0.21 (1966-2013, n=48)	-0.12 (1966-2013, n=48)	<b>0.51</b> (1966-2013, n=48)	<b>0.37</b> (1966-2013, n=48)	0.23 (1966-2013, n=48)
P south*	<b>-0.30</b> (1966-2013, n=48)	<b>0.37</b> (1966-2013, n=48)	-0.13 (1966-2013, n=48)	0.26 (1966-2013, n=48)	0.14 (1966-2013, n=48)	0.25 (1966-2013, n=48)
$\delta^{18}\text{O}$		0.05 (1914-2013, n=100)	0.02 (1914-2013, n=100)	<b>0.41</b> (1914-2013, n=100)	<b>0.41</b> (1950-2013, n=64)	0.19 (1948-2013, n=66)
Accumulation			0.07 (1914-2013, n=100)	-0.18 (1914-2013, n=100)	-0.15 (1950-2013, n=64)	0.18 (1948-2013, n=66)
$d$				-0.06 (1914-2013, n=100)	-0.01 (1950-2013, n=64)	0.11 (1948-2013, n=66)

\*P south – precipitation rate at the weather stations to the South from the Caucasus, P north – precipitation rate at the weather stations to the North from the Caucasus.